

## Article

# Comparison of Spatial Structures and Packaging of Phosphorybosil Pyrophosphate Synthetase 2 from *Thermus thermophilus* HB27 in Rhombohedral and Tetragonal Crystals

Yulia Abramchik <sup>1</sup>, Evgeniy Zayats <sup>1</sup>, Maria Kostromina <sup>1</sup>, Dmitry Lykoshin <sup>1</sup>, Ilya Fateev <sup>1</sup>,  
Irina Konstantinova <sup>1</sup>, Nadezda Zhukhlistova <sup>2</sup>, Vladimir Timofeev <sup>2</sup>, Inna Kuranova <sup>2</sup> and Roman Esipov <sup>1,\*</sup>

<sup>1</sup> Shemyakin and Ovchinnikov Institute of Bioorganic Chemistry, Miklukho-Maklaya Str., 16/10, GSP-7, 117997 Moscow, Russia; ugama@yandex.ru (Y.A.); eaz96post@gmail.com (E.Z.); kostromasha@mail.ru (M.K.); ldd-94@ya.ru (D.L.); ifateev@gmail.com (I.F.); kid1968@yandex.ru (I.K.)

<sup>2</sup> Shubnikov Institute of Crystallography of Federal Scientific Research Centre “Crystallography and Photonics”, Russian Academy of Sciences, Leninskii Prospect 59, 119333 Moscow, Russia; nez@ns.crys.ras.ru (N.Z.); tostars@mail.ru (V.T.); inna@crys.ras.ru (I.K.)

\* Correspondence: esipov@ibch.ru



**Citation:** Abramchik, Y.; Zayats, E.; Kostromina, M.; Lykoshin, D.; Fateev, I.; Konstantinova, I.; Zhukhlistova, N.; Timofeev, V.; Kuranova, I.; Esipov, R. Comparison of Spatial Structures and Packaging of Phosphorybosil Pyrophosphate Synthetase 2 from *Thermus thermophilus* HB27 in Rhombohedral and Tetragonal Crystals. *Crystals* **2021**, *11*, 1128. <https://doi.org/10.3390/cryst11091128>

Academic Editor: Abel Moreno

Received: 4 August 2021

Accepted: 13 September 2021

Published: 16 September 2021

**Publisher's Note:** MDPI stays neutral with regard to jurisdictional claims in published maps and institutional affiliations.



**Copyright:** © 2021 by the authors. Licensee MDPI, Basel, Switzerland. This article is an open access article distributed under the terms and conditions of the Creative Commons Attribution (CC BY) license (<https://creativecommons.org/licenses/by/4.0/>).

**Abstract:** We report the spatial structure of phosphoribosyl pyrophosphate synthetase 2 from the thermophilic bacterium *Thermus thermophilus* HB27 (TthPRPPS2) obtained at a 1.85 Å resolution using a diffraction set collected from rhombohedral crystals (space group  $R3_2-h$ ), grown with lithium sulfate as a precipitant. This crystal structure was compared with the structure of TthPRPPS2, previously obtained at a 2.2 Å resolution using diffraction sets from the tetragonal crystals (space group  $P4_12_12$ ), grown with ammonium sulfate as a precipitant. The comparison of these structures allows the study of the differences between protein molecules in both crystalline structures, as well as the packaging of enzyme molecules in crystals of both spatial groups. Our results may contribute to the research of the structural basis of catalytic activity and substrate specificity of this enzyme.

**Keywords:** phosphoribosyl pyrophosphates; crystalline structure; molecule conformation; intermolecular contacts

## 1. Introduction

Phosphoribosyl pyrophosphate synthetases (PRPPS) catalyze the synthesis of 5-phosphorybosyl- $\alpha$ -1-pyrophosphate (5PRPP), using ribose-5-phosphate (R5P) and ATP as substrates. Enzymes of the PRPPS family are widespread in prokaryotic and eukaryotic organisms [1,2]. The functioning of PRPPS accompanies the most important metabolic processes and is vitally important for a living cell. These enzymes are involved in metabolic processes, including the synthesis of purine and pyrimidine nucleotides, the amino acids histidine and tryptophan, and pyridine coenzymes. PRPP synthetases are the objects of a number of our studies in the multienzymatic cascade conversion of D-pentoses into purine nucleotides [3,4]. One of the ways to improve the cascade and expand the possibilities of its utilization is the use of enzymes with altered substrate specificity.

As mentioned earlier, the product of the PRPPS reaction is PRPP. This molecule is mainly involved in the de novo and salvage biosynthesis of purine and pyrimidine nucleotides and acts as a regulator of both processes [5–7]. The significant role of PRPPS in cellular metabolism requires strict regulation of its activity. The enzyme activity is controlled by two mechanisms: feedback inhibition by excess substrate and allosteric inhibition. The molecule responsible for the latter inhibition mechanism is adenosine diphosphate (ADP), which binds with the allosteric center of the enzyme [8–10].

There are three classes of PRPP synthetases, which are determined by the type of their quaternary structure, the mechanism of regulatory activity, and specificity with respect to the pyrophosphate residue donor [11–13]. The object of research is the thermophilic

enzyme PRPPS2 from *Thermus thermophilus* HB27 (TthPRPPS2). This enzyme belongs to the first-class PRPPS. Enzymes of this subfamily have a hexameric quaternary structure, and their activity depends on phosphate ions and is regulated by allosterically binding ADP or GDF molecules in the allosteric center [14]. Only ATP can serve as the pyrophosphate donor for this class of PRPPS.

Previously, we have obtained the structure of TthPRPPS2 at a resolution of 2.2 Å using protein crystals grown with ammonium sulfate at pH 4.9 as a precipitant [15]. The crystals belonged to the space group  $P4_12_12$ .

In this study, we used a protein solution of the same composition as when growing tetragonal crystals but with lithium sulfate as a precipitant at pH 7.5. This resulted in the growth of the rhombohedral crystals of TthPRPPS2, belonging to the  $R3_2h$  space group. A diffraction set was collected and used to solve the spatial structure of the enzyme at a resolution of 1.85 Å. This study compares the crystal structures of TthPRPPS2 molecules obtained at a resolution of 2.2 and 1.85 Å, and the packing of enzyme molecules in tetragonal and rhombohedral crystals.

## 2. Materials and Methods

The crystals of phosphoribosyl pyrophosphate synthetase 2 from *Thermus thermophilus* HB27 (TthPRPPS2), belonging to space groups  $P4_12_12$  and  $R3_2-h$ , were grown in a capillary under microgravity by the counter diffusion method, as described in [16–18] from protein solutions in 0.02 M Tris-HCl, pH 8.5, containing 1 mM ATP, 1 mM  $MgCl_2$ , 5% Gln, and 0.04%  $NaN_3$ . The protein concentration was 12 mg/mL [15]. When growing tetragonal crystals, 0.8 M ammonium sulfate, 0.45 M KCl, 0.1 M sodium citrate pH 4.9, 5 mM  $MgCl_2$ , 5 mM ATP, and 0.04%  $NaN_3$  were used as precipitants. When growing rhombohedral crystals, 1.7 M lithium sulfate, 0.1 M HEPES pH 7.5, 0.04%  $NaN_3$ , and 5 mM  $MgCl_2$  were used as precipitants.

The spatial structure of tetragonal crystals is described in our previous paper [15] (PDB ID: 5T3O). The spatial structures of both modifications were solved by the molecular replacement method using the Phaser program [19] and *E. coli* PRPPS coordinates (PDB ID: 1DKR) as a starting model [20], for tetragonal crystals (space group  $P4_12_12$ ), and TthPRPPS2 coordinates (PDB ID: 5T3O) as a starting model for rhombohedral crystals [15]. The diffraction set from rhombohedral crystals was collected at a temperature of 100 K at the BL41 station of the SPring-8 synchrotron facility (Japan) at the resolution of 1.85 Å.

The crystal structure (space group  $R3_2-h$ ) was refined at the resolution of 1.85 Å. The refined coordinates (REFMAC program [21]) of the atomic model were deposited in the PDB, PDB\_ID: 7PN0. In both structures, ADP molecules and sulfate ions bounded with the enzyme are localized on the electron density map. The statistics of the X-ray diffraction set and the refinement of the structure are given in Table 1. A fragment of the electron density map is shown in Figure S1.

**Table 1.** Statistical characteristics of the experimental dataset and the results of the refinement of the structure of the rhombohedral TthPRPPS2.

Parameter	Value
Space group	$R3_2-h$
a, c, Å	106.29, 333.29
$\alpha, \gamma, ^\circ$	90, 120
Resolution, Å	20.0–1.85 (1.89–1.85) *
Number of independent reflexes	59412
Completeness, %	100 (99.8)
Redundancy	7.01 (5.96)
I/ $\sigma$ (I)	14.31 (3.53)
$CC_{1/2}$	0.999 (0.905)
R <sub>merged</sub> -F, %	10.5 (54.6)
PDB_ID	7PN0

Table 1. Cont.

Parameter	Value
R <sub>cryst</sub> , %	18.7 (28.5)
R <sub>free</sub> , %	22.1 (31.9)
Number of refined atoms	
Protein	4662
Solvent	257
Ligands	84
Average B-Factor, Å <sup>2</sup>	23.331
rmsd	
Bonds, Å	0.011
Angles, °	1.795
Ramachandran plot	
The most favorable areas	97%
Acceptable areas	3%

\* The brackets include the values for the last shell.

The 5T3O and 7PN0 structures were compared by superposing them with the PyMol program [22]. The analysis of structures, intramolecular, and intermolecular contacts in the crystal structures of TthPRPPS2 was conducted using the PISA web service [23].

### 3. Results and Discussion

The biologically active form of phosphoribosyl pyrophosphate synthetase 2 from *Thermus thermophilus* is homohexamer. The hexamer PRPRS molecule consists of subunits connected by a third-order axis and a second-order axis perpendicular to it and has a point symmetry group of 32.

Rhombohedral and tetragonal crystals of Tth2PRPPS HB27 differ in the number of subunits in the independent part of the unit cell. In the asymmetric unit, tetragonal crystals contain three subunits of a hexameric molecule, and rhombohedral crystals contain two subunits. In tetragonal crystals, the hexamer molecule is formed as a result of the action of the second-order crystallographic axis (the symmetry operator  $y, x, -z$  converts a trimer into a hexamer). In a rhombohedral crystal structure, the third-order symmetry axis of the hexameric molecule coincides with the crystallographic one. A hexamer molecule is formed by applying the symmetry operator  $-y-1, x-y, z$  to two subunits contained in an independent part of the unit cell. In both structures, the point group of pseudosymmetry of the molecule is 32.

Each subunit of the hexameric enzyme molecule consists of two domains: N terminal and C terminal (Figure 1).

Both domains have a polypeptide chain folding characteristic of PRPPS class 1. The polypeptide chain in the N-terminal and C-terminal domains forms a five-stranded  $\beta$ -strand surrounded by four  $\alpha$ -helices. The N-terminal domain additionally contains a  $3_{10}$ -helix and an  $\alpha$ -helix at the C-terminal region. The central core in both domains is covered by a double antiparallel  $\beta$ -layer. These  $\beta$ -layers (turns  $\beta 3$ – $\beta 4$  of the N-terminal domain and  $\beta 9$ – $\beta 10$  of the C-terminal domain) are called flag regions [15]. The domains are bounded by the linker (amino acid residues 147–149). The subunits in the hexameric molecule are stacked similar to a propeller with N-terminal domains at the center of the molecule and C-terminal domains on the surface of the molecule. The active center of the subunit is located in the cavity between the N-terminal and the C-terminal domains. In the N-terminal domain, it is surrounded by the amino acid residues of the flexible loop (Phe92–Ser108) and a fragment of the polypeptide chain of the neighboring subunit (Val30–Ile44). In the C-terminal site, the active center is surrounded by a pyrophosphate-binding site (Asp170–Gly175) and so-called riboso-5-phosphate (R5P) loop (220–228). The flag region of the C-terminal domain containing residues Arg196 and Lys194, which are important for catalytic activity, called catalytic  $\beta$ -hairpin (residues 189–208,  $\beta 9$ – $\beta 10$ ), closes the entrance to the active site during the transition of the enzyme to the closed conformation [15]. In

each subunit of the hexameric enzyme molecule, along with the active center, there is an allosteric center where an ADP molecule can bind [16]. The amino acid residues binding the ADP molecule belong to two adjacent trimer subunits and one of the subunits of the second trimer of the hexameric molecule. For example, tetragonal crystals with three independent subunits A, B, C, forming a trimer, the  $\text{SO}_4$  ion located in the allosteric center of subunit B is coordinated by the amino acid residues of this subunit B, subunit A and subunit C of the second trimer.

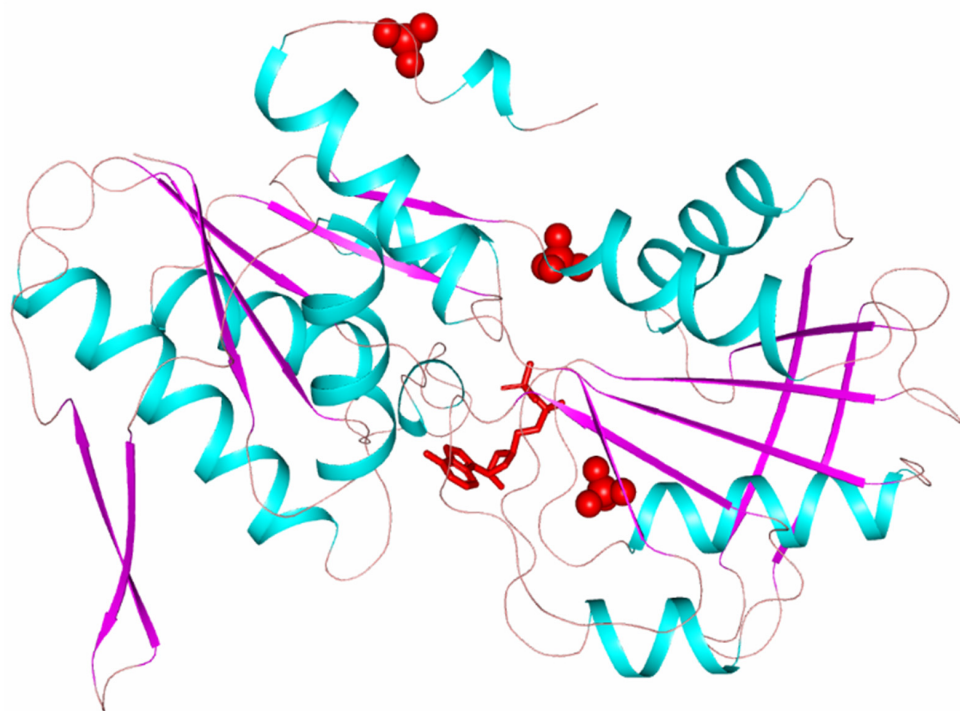


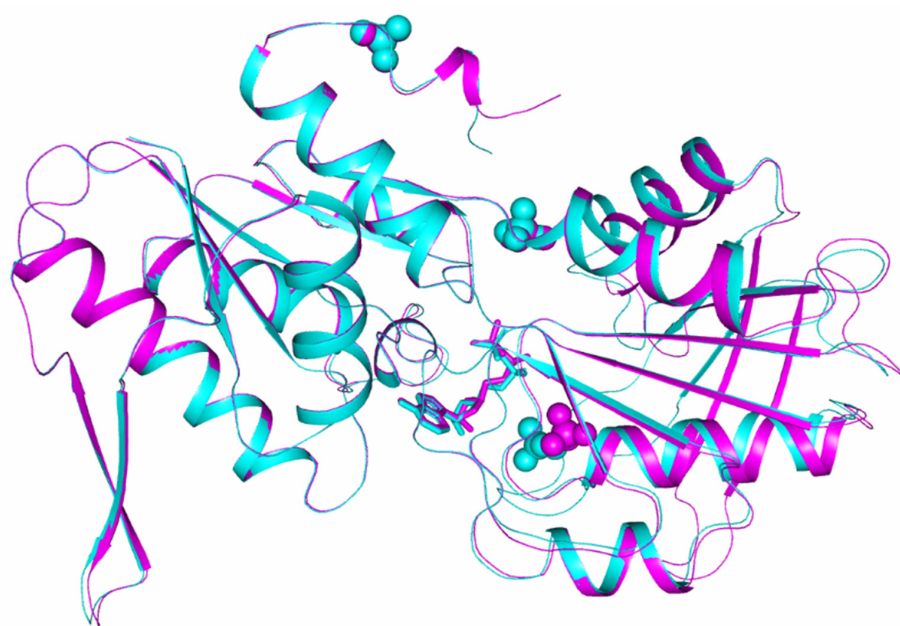
**Figure 1.** TthPRPPS2 subunit polypeptide chain. Red spheres show sulfate ions. The red sticks show the ADP molecule.

In both crystal polymorphs (tetrahedral and rhombohedral), an ADP molecule and a sulfate ion are localized in the active center of each enzyme subunit, and sulfate ions are located in the allosteric centers. An additional  $\text{SO}_4$  ion is localized in rhombohedral crystals, coordinated by amino acid residues Thr129 (loop 128–132), Ser147, Ala148 (irregular region 146–148), and Arg177 ( $\alpha$ -helix 174–186). For the rest of the C $\alpha$  atoms of the subunits, noticeable shifts are observed in the sequences 162–216, 231–244, and in the catalytic hairpin (residues 186–208). In the independent subunits of rhombohedral crystals, the positions of the catalytic hairpins differ and, as a result, the positions of the ligands bounded in these regions: sulfate ions and ADP molecules bounded in the active center. (Figure 2a,b). The positions of sulfate ions, localized in the active centers of independent subunits, differ by 2.6 Å.

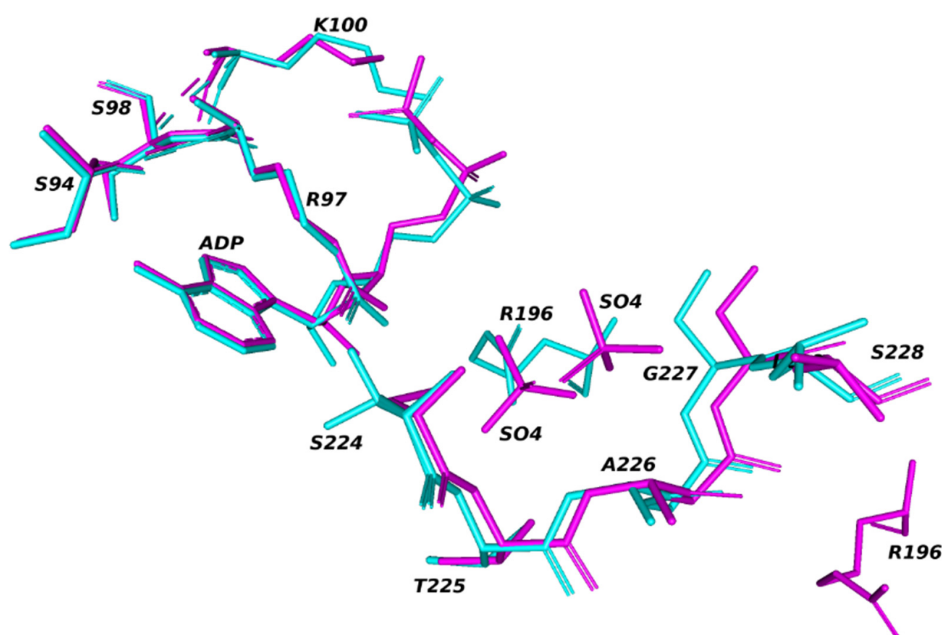
Comparison of the position of the catalytic hairpins showed that in one of the independent subunits (subunit B), the conformation of the active center is more closed (Figure 2a). Thus, the two independent subunits of the molecule have a different conformation of the active center.

Earlier [15], when comparing the conformations of the subunits of the protein molecule in the tetragonal crystal modification, it was found that the catalytic hairpin bounding the active center region has different conformations in three independent TthPRPPS2 subunits, while the closed conformation of the active site was found in one of the subunits. Comparison of conformations of the catalytic loop (residues 188–202) in three independent subunits of tetragonal crystals [15] suggested that different conformations of the catalytic

loop are realized during the transition between the closed and open conformations of the active center.



(a)



(b)

**Figure 2.** Superposition of two independent subunits A and B of the Tth2PRPPS HB27 molecule in rhombohedral crystals. The spheres show sulfate ions. The sticks show the ADP molecule: (a) sulfate ions and ADP molecules in the active centers of superimposed subunits A and B (b).

When subunits with a closed conformation of the active center from different crystal modifications (subunits B with closed conformation in rhombohedral crystals and subunit B with closed conformation in tetragonal crystals) were superimposed over 255 C $\alpha$  atoms, the average rmsd was 0.369 Å (Figure 3).

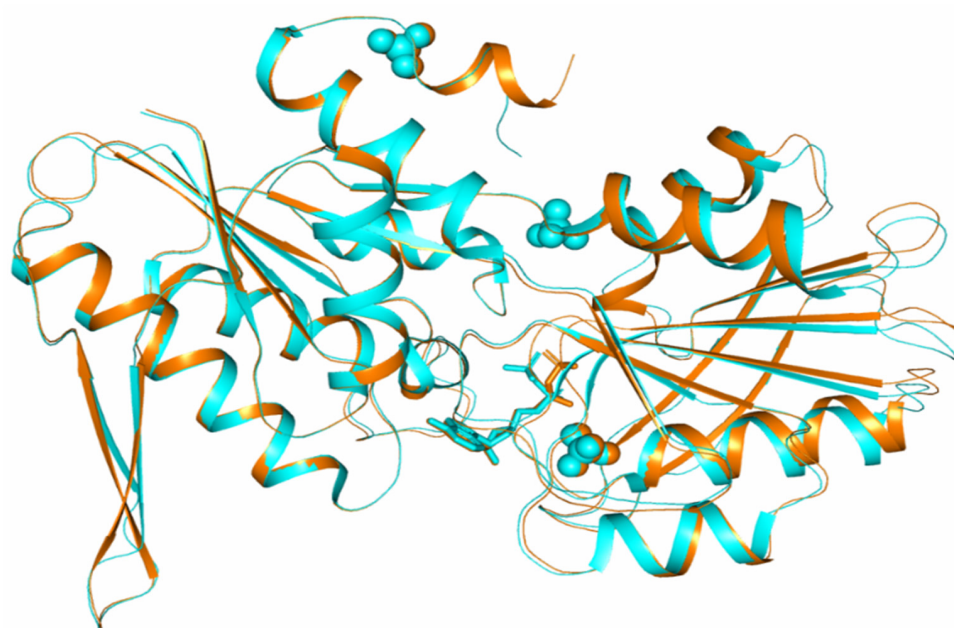


**Figure 3.** Comparison of the conformations of subunits of TthPRPPS2 in two crystal modifications. Subunits superimposed by 255 C $\alpha$  atoms.

The greatest differences were found in the C-terminal domain, where the positions of loops 160–165, 185–189, 208–215, 239–243 differ. All these sites are located on the surface of the molecule. There are also differences in the conformation of some residues of catalytic hairpins ( $\beta 9$ – $\beta 10$ ). Amino acid residues, which are part of the active center of subunits and involved in the coordination of the sulfate ion and the ADP molecule, have the same conformations in the compared subunits of different crystal structures. ADP molecules localized in the active centers of the compared subunits differ in the conformation of phosphate groups (Figure 3).

Intermolecular polar contacts in crystals of two modifications were studied using the PISA program (Table 2). The surface area of enzyme molecules accessible to the solvent is almost the same in both crystalline modifications and amounts to 61040  $\text{\AA}^2$  for tetragonal crystals and 59280  $\text{\AA}^2$  for rhombohedral crystals. However, the number of molecules in the immediate environment and the regions of the polypeptide chain involved in intermolecular interactions are different for both modifications.

As discussed earlier, a trimer is located in the independent part of the tetragonal crystal cell, and a biologically active hexamer molecule is formed under the action of a second-order crystallographic axis (symmetry operator  $y, x, -z$ ). In the tetragonal modification, intermolecular contacts involve molecules bounded by a twofold screw axis, which is parallel to the  $a$  axis at the  $3/8 c$  level (symmetry operator:  $x-1/2, -y-1/2, -z-1/4$ ) (Table 2). Intermolecular contacts with four neighboring molecules form four subunits of a hexamer molecule: independent subunits B, C and subunits B\*, C\* of the second trimer of the molecule, obtained as a result of the action of the symmetry operator  $y, x, -z$ . Hexamer molecule and contacting subunits of other molecules in the  $P4_12_12$  crystal modification are shown in Figure 4.

The total area of contact of one molecule with four neighboring molecules is 3936  $\text{\AA}^2$ . In tetragonal crystals, polar intermolecular interactions involve amino acid residues belonging to the regular regions of the structure: helices  $\alpha 4$ ,  $\alpha 5$ ,  $\eta 4$ , and strand  $\beta 14$  (Table 2).

As mentioned, in rhombohedral crystals, a dimer is located in the independent part of the cell, and a disk-shaped hexamer molecule is formed under the action of a third-order crystallographic axis. In each trimer, the conformation of its subunits is the same, but the conformations of the subunits in different trimers of molecules are different. All six subunits of the hexamer are involved in intermolecular contacts in rhombohedral crystals.

Intermolecular contacts are formed between trimers that have the same conformation of subunits in contacting molecules. The total number of neighboring molecules in contact with the molecule is six. Molecular packing in crystals of the rhombohedral modification is shown in Figure 5.

**Table 2.** Polar contacts between molecules in crystal structures of tetragonal (sp. gr.  $P4_12_12$ ) and rhombohedral (space group  $R3_2-h$ ) modifications.

Tetragonal Crystals, Space Group $P4_12_12$ (PDB_ID: 5T3O)					
Atom (x, y, z)	Secondary Structure Elements	Distance, Å	Atom ( $x-1/2, -y-1/2, -z-1/4$ )	Secondary Structure Elements	
N_THR285/B	$\beta 14$	3.00	O_ALA23/C	$\alpha 1$	
NH1_ARG184/B	$\alpha 5$	3.15	OG1_THR158/C	$\alpha 4$	
ND2_ASN154/B	$\alpha 4$	2.93	O_THR287/C	L	
NH1_ARG284/B	$\beta 14$	2.89	OE1_GLU294/C	$\alpha 8$	
NH2_ARG159/B	$\alpha 4$	3.78	OE2_GLU294/C	$\alpha 8$	
O_SER307/B	$\eta 4$	3.89	NH2_ARG284/C	$\beta 14$	
O_SER307/B	$\eta 4$	3.20	NH1_ARG159/C	$\alpha 4$	
OG_SER307/B	$\eta 4$	3.84	NH2_ARG284/C	$\beta 14$	
O_LEU308/B	$\eta 4$	3.02	NH2_ARG159/C	$\alpha 4$	
Rhombohedral crystals, space group $R3_2 h$ (PDB_ID: 7PN0)					
Atom (x, y, z)	Secondary structure elements	Distance, Å	Atom ( $-x-2/3, -x+y-1/3, -z-1/3$ )	Secondary structure elements	
NH1_ARG159/A	$\alpha 4$	3.99	OE1_GLU303/A	L	
NH1_ARG159/A	$\alpha 4$	3.75	OE2_GLU303/A	L	
NE_ARG284/A	$\beta 14$	3.65	OE1_GLU294/A	$\alpha 8$	
NE_ARG284/A	$\beta 14$	3.17	OE2_GLU294/A	$\alpha 8$	
NH1_ARG284/A	$\beta 14$	3.99	OE1_GLU303/A	L	
NH2_ARG284/A	$\beta 14$	3.23	OE2_GLU294/A	$\alpha 8$	
NH2_ARG284/A	$\beta 14$	3.02	OE1_GLU303/A	L	
OG1_THR285/A	$\beta 14$	3.69	O_ALA23/A	$\alpha 1$	
NH1_ARG298/A	$\alpha 8$	2.84	O_THR158/A	$\alpha 4$	
NH2_ARG298/A	$\alpha 8$	3.17	OG1_THR158/A	$\alpha 4$	
OE2_GLU303/A	L	3.75	NH1_ARG159/A	$\alpha 4$	
OE1_GLU303/A	L	3.99	NH1_ARG159/A	$\alpha 4$	
OE2_GLU294/A	$\alpha 8$	3.17	NE_ARG284/A	$\beta 14$	
OE1_GLU294/A	$\alpha 8$	3.65	NE_ARG284/A	$\beta 14$	
OE2_GLU294/A	$\alpha 8$	3.23	NH2_ARG284/A	$\beta 14$	
OE1_GLU303/A	L	3.99	NH1_ARG284/A	$\beta 14$	
OE1_GLU303/A	L	3.02	NH2_ARG284/A	$\beta 14$	
O_ALA23/A	$\alpha 1$	3.69	OG1_THR285/A	$\beta 14$	
O_THR158/A	$\alpha 4$	2.84	NH1_ARG298/A	$\alpha 8$	
OG1_THR158/A	$\alpha 4$	3.17	NH2_ARG298/A	$\alpha 8$	
Molecules (x, y, z)			Molecule (y, x, -z)		
NH2_ARG298/B	$\alpha 8$	2.83	OD1_ASN154/B	$\alpha 4$	
NE1_TRP297/B	$\alpha 8$	3.30	O_THR158/B	$\alpha 4$	
NE_ARG298/B	$\alpha 8$	3.33	OG1_THR158/B	$\alpha 4$	
NH2_ARG301/B	$\alpha 8$	3.46	O_ARG159/B	$\alpha 4$	
OG1_THR158/B	$\alpha 4$	3.30	OE2_GLU294/B	$\alpha 8$	
OD1_ASN154/B	$\alpha 4$	2.83	NH2_ARG298/B	$\alpha 8$	
O_THR158/B	$\alpha 4$	3.30	NE1_TRP297/B	$\alpha 8$	
OG1_THR158/B	$\alpha 4$	3.33	NE_ARG298/B	$\alpha 8$	
O_ARG159/B	$\alpha 4$	3.46	NH2_ARG301/B	$\alpha 8$	
OE2_GLU294/B	$\alpha 8$	3.30	OG1_THR158/B	$\alpha 4$	

Amino acid residues of helices  $\alpha 4$ ,  $\alpha 8$  participate in polar contacts between subunits B and B\* of neighboring molecules in rhombohedral crystals connected by a twofold axis (symmetry operator  $y, x, -z$ ) (Table 2). Between subunit A of the molecule (x, y, z) and subunit A\* of the molecule associated with the original molecule by the symmetry operator ( $-x-2/3, -x+y-1/3, -z-1/3$ ), twice as many polar contacts exist (Table 2). These contacts are formed by amino acid residues of the same helices and by the residues of helix  $\alpha 1$ , strand  $\beta 14$ , loop 302–306 (Table 2). The total surface area of a molecule in the rhombohedral crystals involved in contacts is  $4215.3 \text{ \AA}^2$ , which exceeds the contact area in a tetragonal structure ( $3936 \text{ \AA}^2$ ). The number of amino acid residues involved in the

contacts of each molecule is 153. The contacts mainly involve the regions of the molecule with an ordered structure (Table 2).

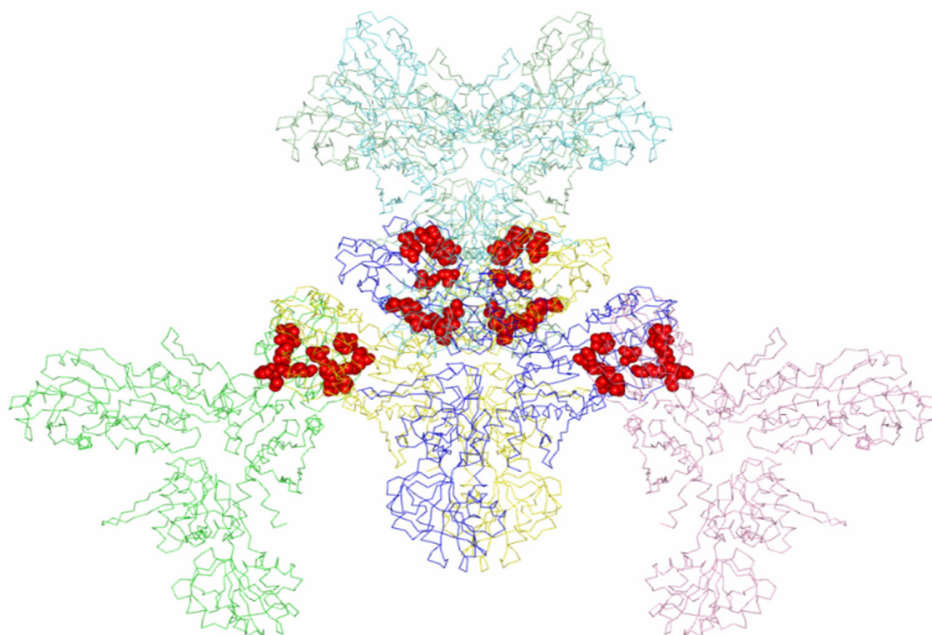


**Figure 4.** Hexameric enzyme molecule and subunits of other molecules in contact with it in the  $P4_12_12$  crystal modification. Amino acid residues involved in intermolecular contacts are shown.

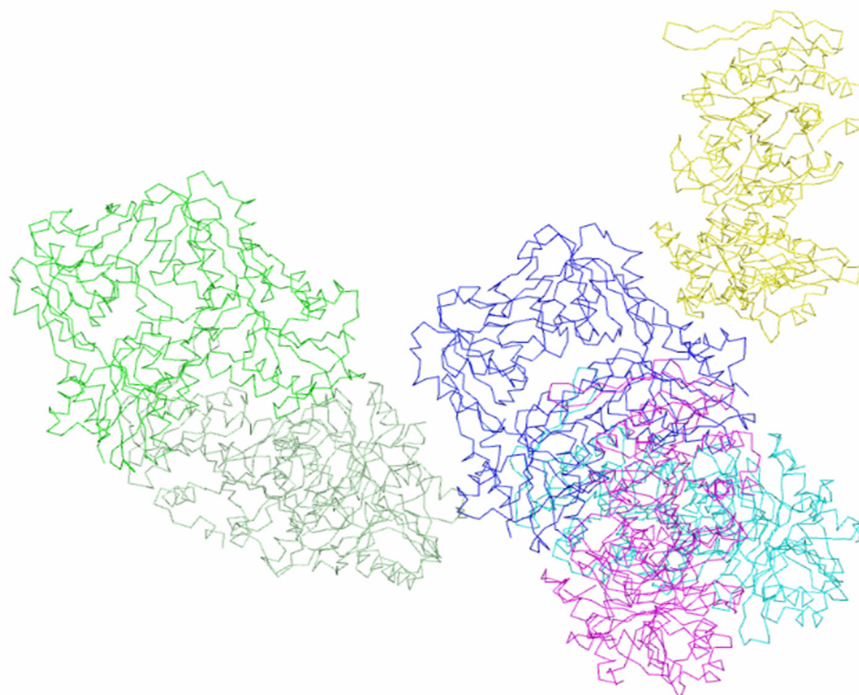


**Figure 5.** Hexameric enzyme molecule and subunits of symmetric related molecules in contact with it in the crystalline modification  $P4_12_12$ .

Figures 6 and 7 show the packing of Tth2PRPPS HB27 molecules in crystal modifications  $P4_12_12$  and  $R3_2-h$ . In the crystal structures of both modifications, there are channels along the  $c$  axis (Figures 6a and 7a). In rhombohedral crystals, such channels are absent, and enzyme molecules in the crystal structure form a layer perpendicular to the  $c$  axis.

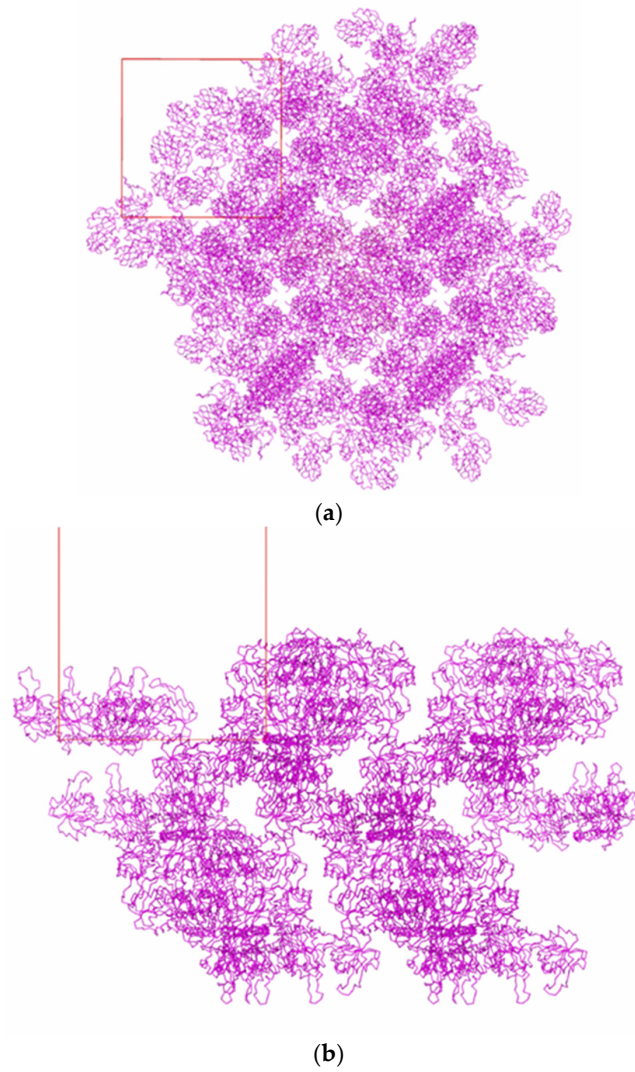


**Figure 6.** Packing of TthPRPPS2 molecules in the  $P4_12_12$  crystal modification: view along the c axis (a); view in the direction perpendicular to the c axis (b).

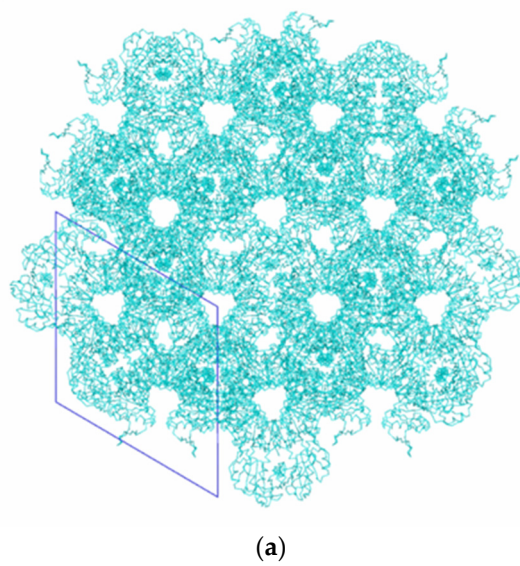


**Figure 7.** Cont.

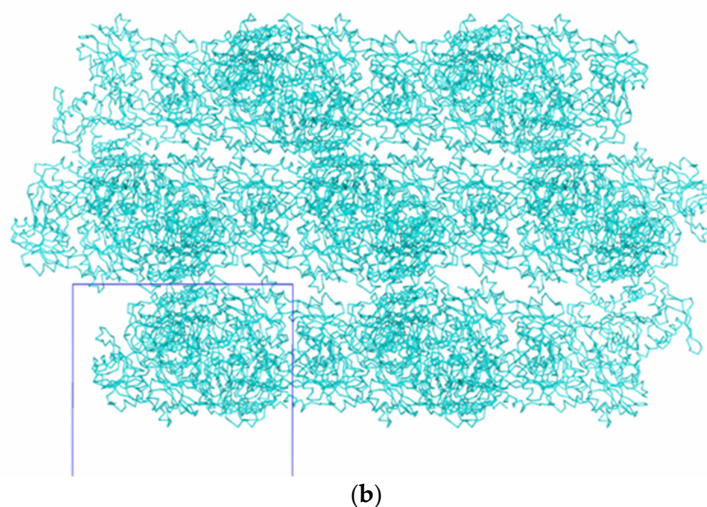


**Figure 7.** Packing of TthPRPPS2 molecules in the  $R3_2h$  crystal modification: view along the  $c$  axis (a); view in the direction perpendicular to the  $c$  axis (b).

Matthews's coefficients [24] for crystal structures belonging to space group  $R3_2h$  and  $P4_12_12$  are 2.73 and 3.52 Å<sup>3</sup>/Da, respectively, which indicates a higher solvent content in the tetragonal structure (65.03%), as compared to the rhombohedral one (55.00%).

Comparison of the spatial structures and conformations of phosphoribosyl pyrophosphate synthetase molecules from the thermophilic bacterium *Thermus thermophilus* HB27, obtained at a resolution of 1.85 Å (rhombohedral crystals of the enzyme, space group  $R3_2h$ ) and at a resolution of 2.2 Å (tetragonal crystals, space group  $P4_12_12$ ), revealed a number of differences. In the rhombohedral crystal modification, the conformation of independent subunits in the region of the active center differs in location and degree of ordering of the catalytic loop, which regulates the degree of openness of the active center. One of the subunits has a closed conformation of the active center, similar to the conformation of one of the subunits in tetragonal crystals.

Analysis of molecular packing in crystal lattices of both space groups and the nature of intermolecular contacts showed that the total surface area of a molecule involved in contacts is larger in rhombohedral crystals. All six subunits of a biological molecule participate in intermolecular interactions in rhombohedral crystals; in tetragonal crystals, intermolecular contacts with neighboring molecules form four subunits of a hexameric molecule. The total number of amino acid residues involved in the intermolecular interactions of each molecule with its neighbors is 153, in rhombohedral crystals, and 134 in tetragonal.

**Supplementary Materials:** The following are available online at <https://www.mdpi.com/article/10.3390/cryst11091128/s1>, Figure S1: The fragment of the electron density map. The 2Fo-Fc is contoured at 2 r.m.s.d.

**Author Contributions:** Conceptualization, V.T. and I.K. (Inna Kuranova); methodology, Y.A., N.Z., V.T., and R.E.; software, V.T.; validation, V.T.; formal analysis, N.Z.; investigation, Y.A., E.Z., M.K., D.L., I.F., I.K. (Irina Konstantinova), N.Z., V.T., I.K. (Inna Kuranova), and R.E.; resources, I.K. (Inna Kuranova) and R.E.; data curation, Y.A., M.K., D.L., I.F., I.K. (Irina Konstantinova), N.Z., and V.T.; writing—original draft preparation, N.Z.; writing—review and editing, Y.A., E.Z., M.K., V.T., I.K. (Inna Kuranova), and R.E.; visualization, V.T.; supervision, R.E.; project administration, R.E.; funding acquisition, R.E. All authors have read and agreed to the published version of the manuscript.

**Funding:** This research was funded by the Russian Science Foundation (project No. 21-13-00429) and the Ministry of Science and Higher Education within the State assignment FSRC “Crystallography and Photonics” RAS in part of collection of X-ray diffraction datasets for financial support of this work.

**Data Availability Statement:** Not applicable.

**Conflicts of Interest:** The authors declare no conflict of interest.

## References

1. Switzer, R.L. Regulation and mechanism of phosphoribosylpyrophosphate synthetase. I. Purification and properties of the enzyme from *Salmonella typhimurium*. *J. Biol. Chem.* **1969**, *244*, 2854–2863. [\[CrossRef\]](#)
2. Becker, M.A.; Raivio, K.O.; Bakay, B.; Adams, W.B.; Nyhan, W.L. Variant human phosphoribosylpyrophosphate synthetase altered in regulatory and catalytic functions. *J. Clin. Investig.* **1980**, *65*, 109–120. [\[CrossRef\]](#) [\[PubMed\]](#)
3. Esipov, R.S.; Abramchik, Y.A.; Fateev, I.V.; Konstantinova, I.D.; Kostromina, M.A.; Muravyova, T.I.; Artemova, K.G.; Miroshnikov, A.I. A Cascade of Thermophilic Enzymes As an Approach to the Synthesis of Modified Nucleotides. *Acta Nat.* **2016**, *8*, 82–90. [\[CrossRef\]](#)
4. Fateev, I.V.; Kostromina, M.A.; Abramchik, Y.A.; Eletskaia, B.Z.; Mikheeva, O.O.; Lukoshin, D.D.; Zayats, E.A.; Berzina, M.Y.; Dorofeeva, E.V.; Paramonov, A.S.; et al. Multi-Enzymatic Cascades in the Synthesis of Modified Nucleosides: Comparison of the Thermophilic and Mesophilic Pathways. *Biomolecules* **2021**, *11*, 586. [\[CrossRef\]](#) [\[PubMed\]](#)
5. Hove-Jensen, B. Mutation in the phosphoribosylpyrophosphate synthetase gene (prs) that results in simultaneous requirements for purine and pyrimidine nucleosides, nicotinamide nucleotide, histidine, and tryptophan in *Escherichia coli*. *J. Bacteriol.* **1988**, *170*, 1148–1152. [\[CrossRef\]](#) [\[PubMed\]](#)
6. Hove-Jensen, B. Phosphoribosylpyrophosphate (PRPP)-less mutants of *Escherichia coli*. *Mol. Microbiol.* **1989**, *3*, 1487–1492. [\[CrossRef\]](#)
7. Hove-Jensen, B.; Nygaard, P. Phosphoribosylpyrophosphate synthetase of *Escherichia coli*, Identification of a mutant enzyme. *Eur. J. Biochem.* **1982**, *126*, 327–332. [\[CrossRef\]](#) [\[PubMed\]](#)
8. Switzer, R.L.; Sogin, D.C. Binding of the substrates and the allosteric inhibitor adenosine 5'-diphosphate to phosphoribosylpyrophosphate synthetase from *Salmonella typhimurium*. *J. Biol. Chem.* **1973**, *248*, 1063–1073. [\[CrossRef\]](#)
9. Becker, M.A.; Kostel, P.J.; Meyer, L.J. Human erythrocyte phosphoribosylpyrophosphate synthetase. Subunit analysis and states of subunit association. *J. Biol. Chem.* **1975**, *250*, 6822–6830. [\[CrossRef\]](#)
10. Gibson, K.J.; Schubert, K.R.; Switzer, R.L. Binding of the substrates and the allosteric inhibitor adenosine 5'-diphosphate to phosphoribosylpyrophosphate synthetase from *Salmonella typhimurium*. *J. Biol. Chem.* **1982**, *257*, 2391–2396. [\[CrossRef\]](#)
11. Krath, B.N.; Hove-Jensen, B. Implications of secondary structure prediction and amino acid sequence comparison of class I and class II phosphoribosyl diphosphate synthetases on catalysis, regulation, and quaternary structure. *Protein Sci.* **2001**, *10*, 2317–2324. [\[CrossRef\]](#)
12. Li, S.; Lu, Y.; Peng, B.; Ding, J. Crystal structure of human phosphoribosylpyrophosphate synthetase 1 reveals a novel allosteric site. *Biochem. J.* **2007**, *401*, 39–47. [\[CrossRef\]](#)
13. Kadziola, A.; Jepsen, C.H.; Johansson, E.; McGuire, J.; Larsen, S.; Hove-Jensen, B. Novel class III phosphoribosyl diphosphate synthetase: Structure and properties of the tetrameric, phosphate-activated, non-allosterically inhibited enzyme from *Methanocaldococcus jannaschii*. *J. Mol. Biol.* **2005**, *354*, 815–828. [\[CrossRef\]](#)
14. Esipov, R.S.; Abramchik, Y.A.; Fateev, I.V.; Muravyova, T.I.; Artemova, K.G.; Konstantinova, I.D.; Kuranova, I.P.; Miroshnikov, A.I. Recombinant phosphoribosyl pyrophosphate synthetases from *Thermus thermophilus* HB27: Isolation and properties. *Bioorg. Chem.* **2016**, *42*, 512–521. [\[CrossRef\]](#)
15. Timofeev, V.I.; Sinitsyna, E.V.; Kostromina, M.A.; Muravieva, T.I.; Makarov, D.A.; Mikheeva, O.O.; Kuranova, I.P.; Esipov, R.S. Crystal structure of recombinant phosphoribosylpyrophosphate synthetase 2 from *Thermus thermophilus* HB27 complexed with ADP and sulfate ions. *Acta Cryst.* **2017**, *F73*, 369–375. [\[CrossRef\]](#)
16. Timofeev, V.I.; Smirnova, E.A.; Chupova, L.A.; Esipov, R.S.; Kuranova, I.P. X-ray study of the conformational changes in the molecule of phosphopantetheine adenylyltransferase from *Mycobacterium tuberculosis* during the catalyzed reaction. *Acta Cryst.* **2012**, *D68*, 1660–1670. [\[CrossRef\]](#)
17. Takahashi, S.; Tsurumura, T.; Aritake, K.; Furubayashi, N.; Sato, M.; Yamanaka, M.; Hirota, E.; Sano, S.; Kobayashi, T.; Tanaka, T.; et al. High-quality crystals of human haematopoietic prostaglandin D synthase with novel inhibitors. *Acta Cryst.* **2010**, *F66*, 846–850. [\[CrossRef\]](#) [\[PubMed\]](#)
18. Kuranova, I.P.; Smirnova, E.A.; Abramchik, Y.A.; Timofeev, V.I.; Kovalchuk, M.V.; Chupova, L.A.; Esipov, R.S.; Akparov, V.K. Crystal growth of phosphopantetheine adenylyltransferase, carboxypeptidase t, and thymidine phosphorylase on the international space station by the capillary counter-diffusion method. *Crystallogr. Rep.* **2011**, *56*, 884–891. [\[CrossRef\]](#)
19. McCoy, A.J.; Grosse-Kunstleve, R.W.; Adams, P.D.; Winn, M.D.; Storoni, L.C.; Read, R.J.J. Phaser (CCP4: Supported Program) NAME phaser-2.5. 0-Maximum Likelihood Analysis and Phasing. SYNOPSIS phaser. *Appl. Cryst.* **2007**, *40*, 658–674. [\[CrossRef\]](#) [\[PubMed\]](#)
20. Eriksen, T.A.; Kadziola, A.; Bentsen, A.K.; Harlow, K.W.; Larsen, S. Structural basis for the function of *Bacillus subtilis* phosphoribosyl-pyrophosphate synthetase. *Nat. Struct. Biol.* **2000**, *7*, 303–308. [\[CrossRef\]](#)
21. Murshudov, G.N.; Skubák, P.; Lebedev, A.A.; Pannu, N.S.; Steiner, R.A.; Nicholls, R.A.; Winn, M.D.; Long, F.; Vagin, A.A. REFMAC5 for the refinement of macromolecular crystal structures. *Acta Cryst.* **2011**, *D67*, 355–367. [\[CrossRef\]](#) [\[PubMed\]](#)
22. Schrodinger, L.L.C. *The PyMOL Molecular Graphics System*; Version 1.8; Schrodinger, L.L.C.: New York, NY, USA, 2015.
23. Krissinel, E.; Henrick, K. Inference of macromolecular assemblies from crystalline state. *J. Mol. Biol.* **2007**, *372*, 774–797. [\[CrossRef\]](#) [\[PubMed\]](#)
24. Matthews, B.W. Solvent content of protein crystals. *J. Mol. Biol.* **1968**, *33*, 491–497. [\[CrossRef\]](#)